Charged particle pseudorapidity distributions in nucleus-nucleus collisions from SPS to LHC

Francesco Prino, INFN sezione di Torino

Abstract

Pseudorapidity distributions of charged particles produced in heavy ion collisions are a powerful tool to characterize the global properties of the created system. They have been measured in a wide range of energies at the GSI, AGS, SPS and RHIC accelerators and will be one of the first measurements at ALICE at the LHC. The various analysis techniques developed by SPS and RHIC experiments are reviewed and the presently available results from SPS and RHIC are presented, focusing in particular on the scaling of charged particle yield with centrality and with center-of-mass energy. Finally the perspectives for the multiplicity measurement in the ALICE experiment at the LHC are discussed.

1 Introduction

Heavy-ion collisions are the experimental tool used to study nuclear matter under extreme temperature and density conditions. The total number of particles produced in these collisions (multiplicity) is a global variable that is essential for their characterization, because it quantifies to which extent the incoming beam energy is released to produce new particles. Particle multiplicity contains information about the entropy of the system and the gluon density in the first stages of the collision evolution. Furthermore, it is related to the impact parameter, i.e. to the centrality of the collision: more particles are produced in central (small impact parameter, many elementary nucleon-nucleon collisions) than in peripheral reactions.

Since experimental detection methods are usually sensitive to ionizing (charged) particles, it is useful to introduce the charged multiplicity ($N_{\rm ch}$) of the collision defined as the total number of charged particles produced in the interaction.

The measurement of charged multiplicity as a function of the energy ($\sqrt{s}$) and the centrality of the collision may help constrain different models of particle production, and estimate the relative importance of soft versus hard processes in the particle production mechanisms at different energies. Hard parton-parton scatterings with large momentum transfer occur on a short time scale and are governed by perturbative QCD; they are expected to scale like the number of elementary nucleon-nucleon collisions ($N_{\rm coll}$). The bulk of particle production occurs via soft processes (with low momentum transfer and consequently longer time-scales) which are described with phenomenological models and predicted to scale with the number of participant nucleons ($N_{\rm part}$) [1].

The values of $N_{\rm part}$ and $N_{\rm coll}$ as a function of the collision impact parameter are usually evaluated by means of Glauber model calculations [2]. An example of such calculations for Pb-Pb collisions and different values of the nucleon-nucleon inelastic cross-sections is shown in fig. 1. It can be seen (left panel) that $N_{\rm part}$ does not change significantly from AGS
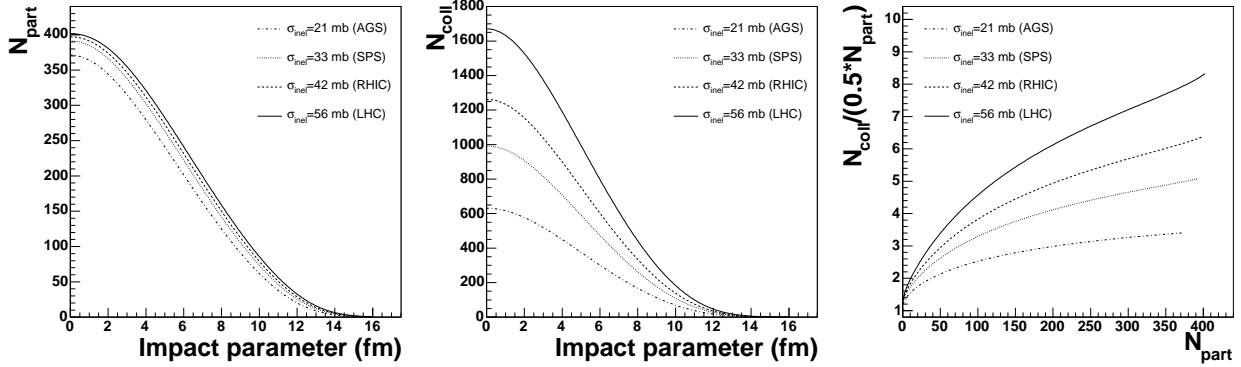
Figure 1: N_{part} (left) and N_{coll} (middle) as a function of impact parameter b for different values of nucleon-nucleon inelastic cross-section. In the right panel, the number of collisions per participant pair as a function of N_{part} is shown.

to LHC energies, meaning that the system volume is almost independent of energy. On the contrary N_{coll} (middle panel), being proportional to the nucleon-nucleon inelastic cross-section, increases dramatically with increasing energy, leading to the expectation that the higher the collision energy, the more important the contribution from hard processes.

From the right plot in fig. 1 it can be seen that the number of collisions per participant pair (which governs the balance between hard and soft processes), increases both with the centrality (N_{part}) and the energy of the collision.

A deeper insight into particle production mechanisms can be obtained from particle momenta distributions. Particle momenta are usually decomposed in the component transverse to the beam axis (p_{T}) and in the one along the beam axis (p_{L}). In this way, all the information about the velocity of the particle-emitting source is contained in the longitudinal momentum, while the transverse momentum is free from kinematic effects and is governed only by the internal characteristics of the system which emits the particles.

To study the longitudinal expansion it is convenient to use the rapidity $y = \frac{1}{2} \ln \frac{E + p_L}{E - p_L}$ and pseudorapidity $\eta = -\ln\left[\tan\left(\vartheta/2\right)\right]$ variables, the latter being an approximation of the rapidity for large momentum particles. Pseudorapidity is more easily accessed experimentally because it requires to measure only one kinematic quantity for each particle, i.e. the angle ϑ of relative to the beam axis.

In the following, pseudorapidity distribution of unidentified charged particles will be discussed. Since this measurement does not require momentum measurement and particle identification capabilities, it is a typical first-day observable in heavy-ion experiments. Nevertheless, the following interesting physical issues can be addressed by studying these distributions:

1. The mid-rapidity region which is populated by particles with $p_{\mathrm{T}} > p_{\mathrm{L}}$ ($p_{\mathrm{T}} = p_{\mathrm{L}}$ corresponds to $\eta = \pm 0.88$) is especially sensitive to the details of the hadroproduction mechanisms. The pseudorapidity density of charged particles at mid-rapidity ($dN/dy\,|_{\mathrm{y=y_{cm}}}$ or $dN/d\eta\,|_{\mathrm{max}}$) is commonly used to characterize the multiplicity of particles produced

2

in the reaction because it allows a comparison between different experiments, being independent of the detailed phase-space acceptance. Furthermore, under the assumption of a boost-invariant central plateau, it can be used to estimate the energy density reached in the collision using the Bjorken formula [3]:

$$\varepsilon_{BJ} = \frac{< m_T >}{\mathcal{A}c\tau_o} \left(\frac{dN}{dy}\right)_{y=y_{cm}} \tag{1}$$

2. The width of the pseudorapidity distributions contains information about the longitudinal expansion of the system and the degree of stopping (transparency) which characterizes the reaction. In the case of two nuclei that completely stop each other giving rise to a baryon-rich fireball, a single isotropic source emitting at rest should be observed and the $dN_{ch}/d\eta$ distributions should present a typical $1/\cosh^2 \eta$ shape, with a FWHM of 1.72 pseudorapidity units.

3. The forward and backward regions where $p_{L} >> p_{T}$ (close to beam rapidities) allow to investigate effects connected with projectile and target fragmentation, with particular attention to the issue of "limiting fragmentation" [4].

2   Experimental issues

Different analysis techniques have been developed by various experiments to extract the $dN_{ch}/d\eta$ distributions of charged particles. In the following, a brief review of the methods used by SPS and RHIC experiments is given.

A first method, typically used with detectors with high segmentation and binary readout (only hit/no hit information for each channel), consists in counting fired channels (hits). Analyses based on this method have been performed by NA50 [5] at SPS and PHOBOS [6] at RHIC. Generally, one hit on a detector is not necessarily equal to one crossing particle because of multiple occupancy (two or more particles hitting the same sensitive element) and clustering effects which cause the signal of one particle to extend to more than one detector channel. Multiple occupancy can be reduced by increasing the detector segmentation so as to keep the channel occupancy below a confidence level. Clustering effects can occur both due to physical processes (such as inclined tracks, charge sharing between contiguous sensitive elements) and to electronic effects (noise, cross-talk between electronic channels...). Hence, in experimental analyses based on detectors with binary readout, clusters (i.e. groups of contiguous channels firing together) are counted and a correction to account for multiple occupancy in a cluster is applied. As an example, NA50 reported [5] that a Monte Carlo simulation, which contains a complete description of their experimental setup and only clustering mechanisms of physical origin, is not able to reproduce the cluster-size distributions observed on their silicon microstrip detector. Probabilities for clustering mechanisms were therefore included in the simulations so as to fit the measured cluster-size distributions and to extract the number of incident particles.

If the detector readout stores the signal amplitudes, thus providing a measurement of energy deposition in each channel, the number of crossing particles can be calculated from the signal recorded in each channel divided by the average energy loss of a typical particle. Particular attention has to be used when dealing with thin detectors (such as silicon strip detectors), where the energy deposition follows a Landau distribution and a correction for particles depositing much more energy than the most probable value has to be included in the analysis. This method has been used by NA57 [7] at SPS and PHOBOS [6] and BRAHMS [8, 9] at RHIC.

A more refined method can be used when two planes of highly segmented detectors are present. This method was first introduced by PHOBOS experiment [10] and consists in associating hits on two detector planes and building a so-called tracklet. The association is normally done by considering straight line tracks departing from the primary vertex which is therefore required to be known. A similar method has also been used by PHENIX [11] experiment. Compared to the previous single-plane methods, tracklets allow a more powerful background rejection but require more precision in detector alignment and knowledge of the primary vertex.

Finally, a method based on full track reconstruction has been used by experiments with large tracking detectors, such as NA49 [12] and STAR [13]. This is the most powerful method, which is normally accompanied by momentum measurement and particle identification, thus allowing to measure rapidity distributions of the various particle species.

A correction for secondary production in material placed upstream of the detector plane has to be applied, especially in the case of analyses based on single plane measurement. This correction is usually extracted from Monte Carlo simulations of the experimental apparatus. In the case of NA50, for example, the secondary/primary ratio is reported to be of the order of 1.2-1.8 [5], mainly due to the Pb target thickness. The analyses based on tracking require a Monte Carlo correction to take into account tracking efficiency and, if a magnetic field is present, low p_{T} particle cut-off.

3   Experimental results from SPS and RHIC

In the following sections some of the presently available experimental results from SPS and RHIC accelerators are discussed, focusing on the centrality dependence at a given energy and on the energy dependence observed for the most central collisions. First the pseudorapidity density of charged particles at mid-rapidity are presented. Then, measurements of the width of the $dN_{\mathrm{ch}}/d\eta$ distributions are reviewed. Subsequently, the main features observed in the fragmentation regions, with particular attention to the limiting fragmentation behaviour are described. Finally, the total yield of charged particles is discussed.
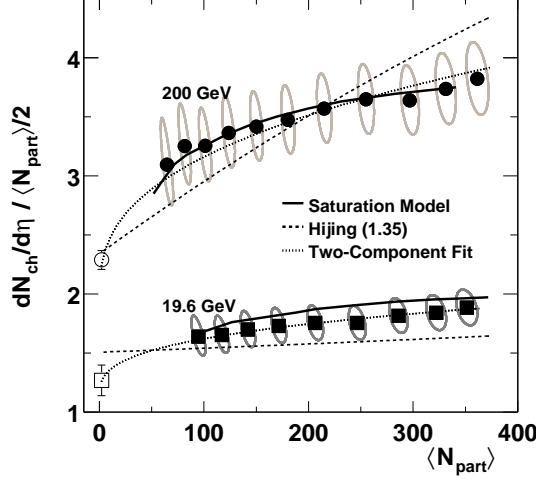
Figure 2: Mid-rapidity pseudorapidity density per participant pair as a function of centrality as measured by PHOBOS experiment at $\sqrt{s}$=19.6 and 200 GeV (taken from [17])

3.1 Particle yield at mid-rapidity

3.1.1 Scaling with centrality

The scaling of pseudorapidity density of charged particles at mid-rapidity as a function of centrality is an important test for models of particle production in heavy ion reactions because it allows to quantify the relative importance of soft ($\propto N_{\mathrm{part}}$) and hard ($\propto N_{\mathrm{coll}}$) processes.

SPS experiments typically performed $N_{\mathrm{part}}{}^{\alpha}$ fits to the measured $dN/d\eta \mid_{\mathrm{max}}$ in different centrality bins. Values of α ranging in the range from 1.00 (NA50 [14]) to 1.08 (WA98 [15]) have been found. This is usually understood as an indication that hard scatterings do not play an appreciable role at such energies. It has to be stressed that the value of α depends on the model used to calculate N_{part}, which is not a direct experimental observable. For example, NA50 quoted $\alpha = 1.00$ when N_{part} is extracted from a Glauber calculation in the optical approximation and $\alpha = 1.08$ when a Monte Carlo generator (VENUS [16]) is used.

A convenient variable to be used in such studies is the particle yield per participant pair at mid-rapidity, defined as $dN/d\eta \mid_{\mathrm{max}}/(N_{\mathrm{part}}/2)$. At SPS energies this quantity is found to be rather flat as a function of centrality, reflecting the approximate scaling with N_{part} of the multiplicity at mid-rapidity.

At RHIC energies ($\sqrt{s} = 20 - 200$ GeV) a clear increase is observed in the $dN/d\eta \mid_{\mathrm{max}}$ per participant pair with increasing centrality, as it can be seen in fig. 2. The normalized yield at mid-rapidity increases by $\approx 25\%$ from mid-peripheral to central collisions. Early theoretical explanations attributed this increase to the contribution of hard processes in particle production, which grows with increasing centrality. However, this explanation is challenged by the observed fact that the ratio of the measured $dN/d\eta \mid_{\mathrm{max}}$ per participant

pair at the two energies is almost independent of centrality, while the contribution from hard processes should lead to a stronger centrality dependence with increasing collision energy, as it is illustrated by the HIJING [18] prediction shown in fig. 2. This consideration is also supported by the results of fits to the data points in fig. 2 with a simple two-component parametrization [19]:

$$\frac{dN_{ch}}{d\eta} = n_{pp}\left((1-x)\frac{< N_{part} >}{2} + x < N_{coll} >\right) \tag{2}$$

The parameter x, representing the fraction of hard process, is found to be consistent at both energies with a single value $x = 0.13 \pm 0.01 \pm 0.05$ [17]. The RHIC data about particle yields at mid-rapidity are described rather well by models based on parton saturation [19, 20], indicating that high density QCD effects probably play an important role in determining the global event features at RHIC energies. However, as pointed out in [21], different models to calculate N_{part} (which is not a direct experimental observable and affects both axes of fig. 2) would lead to different slopes for the centrality dependence of the $dN/d\eta\mid_{\mathrm{max}}$ per participant pair, thus weakening the relevance of parton saturation and Color Glass Condensate in the initial state of RHIC collisions. By the way, differences in N_{part} calculation may explain also why the yield per participant pair is found to be almost flat as a function of centrality at $\sqrt{s}$=17.2 GeV by SPS experiments and increasing with centrality by PHOBOS at the very similar energy of $\sqrt{s}$=19.6 GeV.

3.1.2   Scaling with energy

Important information can be extracted analyzing the pseudorapidity density of charged particles at mid-rapidity for central events as a function of the center-of-mass energy of the collision. When comparing the $dN/d\eta\mid_{\mathrm{max}}$ values between fixed-target and collider experiments, it should be taken into account that $dN_{\mathrm{ch}}/d\eta$ (contrarily to dN_{ch}/dy) distributions are not boost invariant and therefore the value at the peak differs if measured in the laboratory or in the center-of-mass frame. So, data measured in the laboratory frame should be converted into the Lorentz invariant dN_{ch}/dy and then back to the $dN_{\mathrm{ch}}/d\eta$ in the center-of-mass using the formula:

$$\frac{dN_{ch}}{d\mathbf{p}_T d\eta} = \sqrt{1 - \frac{m^2}{m_T^2\cosh^2 y}}\ \frac{dN_{ch}}{d\mathbf{p}_T dy} \tag{3}$$

The scaling of $dN/d\eta\mid_{\mathrm{max}}$ per participant pair as a function of $\sqrt{s}$ for central heavy-ion collisions from AGS to RHIC energies is shown in fig 3 together with the same quantity as measured in proton-proton collisions. It is immediately seen that nucleus-nucleus collisions can not be explained as an incoherent superposition of nucleon-nucleon interactions. The multiplicity per participant pair in nucleus-nucleus collisions is in agreement with the one measured in pp($\bar{\mathrm{p}}$) reactions only at AGS energies. In the SPS energy range a departure from the proton-(anti)proton trend is observed and more particles per participant pair are produced at mid-rapidity in nuclear collisions with respect to proton collisions at the same energy. The measured multiplicities appear to fall on a smooth curve from AGS to top
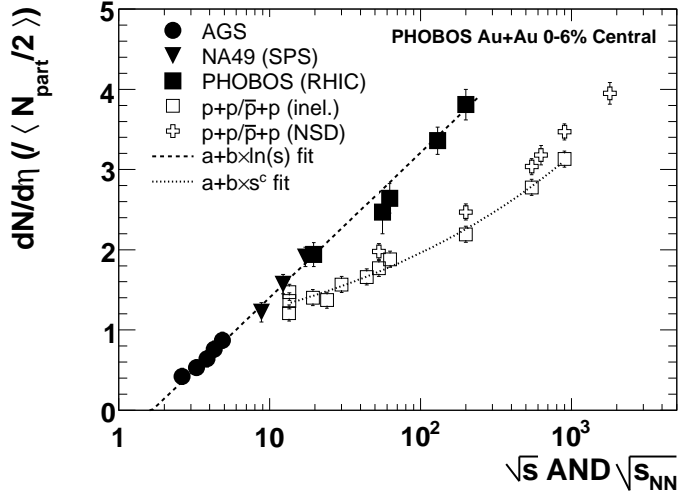
Figure 3: Energy dependence of the pseudorapidity density of charged particles per participant pair (in the center-of-mass frame) for the most central ion-ion collisions from AGS to RHIC (taken from [22]). pp(p̄) data are superimposed.

RHIC energies and this result contrasts with some theoretical predictions made before RHIC startup, which were suggesting strong energy dependences accompanying the hadron to QGP phase transition.

Starting from the measured values of $dN/d\eta \mid_{\mathrm{max}}$ an estimation of the energy density attained in central Au-Au collisions at top RHIC energy can be performed using the Bjorken formula:

$$\varepsilon_{BJ} = \frac{<m_T>}{\mathcal{A}c\tau_o}\left(\frac{dN}{dy}\right)_{y=y_{cm}} \approx \frac{0.6\mathrm{GeV/c^2}}{145\mathrm{fm^2}\times c\times\tau_o}\times\left(700\times\frac{3}{2}\times 1.1\right) \quad (4)$$

where the factor 3/2 accounts for neutral particles and the factor 1.1 for the difference between $dN_{\mathrm{ch}}/d\eta$ and dN_{ch}/dy. Depending on the value assumed for τ_o, i.e. on the instant when the energy density is evaluated, different values of ε are obtained. At the formation time $\tau_f = \hbar/ < m_T >\approx 0.35$ fm/c [23] the energy density would be ≈ 15 GeV/fm³. At the instant $\tau = 0.6 - 1$ fm/c, which is the time estimated for the system to reach local thermal equilibrium, the energy density would be $\approx$5-9 GeV/fm³. It is clear that, also for the more conservative choice for τ_o, the estimated energy density for Au-Au collisions at $\sqrt{s}$=200 GeV is well above the one predicted by lattice QCD calculations for the phase transition to QGP.

3.2   Width of the distribution

3.2.1   Scaling with centrality

A decrease of the width of the $dN_{\mathrm{ch}}/d\eta$ distributions (expressed as gaussian width or FWHM) with increasing collision centrality has been observed by several experiments at various ener-
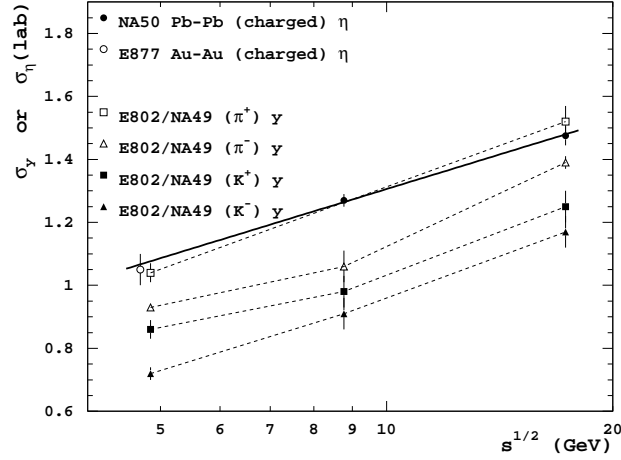
Figure 4: Energy dependence of the width of gaussian fits to pseudorapidity and rapidity distributions at AGS and SPS energies (taken from [14]).

gies, among which E802 [24] at the AGS, NA50 [14] at two SPS energies and PHOBOS [25] at RHIC. This narrowing can be associated with the higher degree of stopping reached in the interaction, and it is mostly due to the decreasing contribution of protons from target and projectile fragmentation. In fact, emulsion experiments, which report the distribution of shower particles ($\beta > 0.7$) excluding therefore slow protons from the target fragmentation, usually find a weaker dependence of σ_η on centrality (see e.g. [26]).

3.2.2   Scaling with energy

The width of the gaussian fits performed to $dN_{\rm ch}/d\eta$ ($dN_{\rm ch}/dy$) distributions in central collisions at SPS and AGS energies as a function of $\sqrt{s}$ is shown in fig. 4. It can be seen that the width increases with increasing $\sqrt{s}$ reflecting the fact that the available phase space in rapidity increases with the center-of-mass energy, following a simple logarithmic scaling law ($\sigma_\eta = a + b \times \ln \sqrt{s}$) independent of system size. .The same scaling is observed also for the widths of the rapidity distributions for identified produced hadrons with $\sigma_\eta \approx \sigma_y(\pi^+)$ and $\sigma_y(\pi^+) > \sigma_y(\pi^-) > \sigma_y(K^+) > \sigma_y(K^-)$.

Finally, it is interesting to note [27] that at 158 GeV/nucleon the width of the rapidity distributions is about twice as large as the one expected from a single thermal source located at mid-rapidity.

3.3   Fragmentation regions

Taking advantage of its large pseudorapidity coverage, PHOBOS experiment studied particle production in the fragmentation regions of the colliding nuclei, so as to investigate the
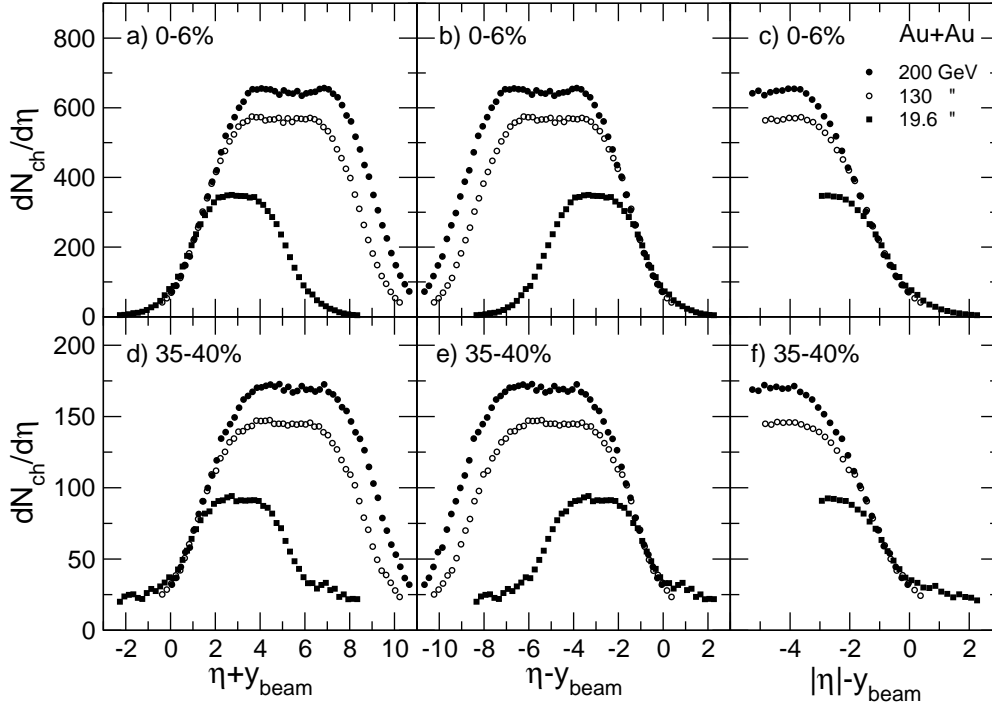
Figure 5: Pseudorapidity distributions of charged particles in Au-Au collisions at $\sqrt{s}$=19.6, 130 and 200 GeV and two centrality ranges in the rest frames of the two colliding nuclei (taken from [28]).

limiting fragmentation hypothesis [4]. For this analysis, it is convenient to consider the particle distributions in the rest frame of one of the two colliding nuclei by introducing the variables $y' = y - y_{beam}$ and $\eta' = \eta - y_{beam}$. The limiting fragmentation ansatz states that at high enough collision energy, both $d^2N/dy'dp_T$ and the mix of particle species reach a limiting value and become energy independent in a region around $y' = 0$. In particular, this effect implies also a limiting value for $dN/d\eta'$ which is expected to be energy independent in a region around $\eta' = 0$.

The results obtained by PHOBOS [25] in Au-Au collisions at three different energies are shown in fig. 5. The distributions follow a common limiting curve independent of collision energy over a wide η' range. Furthermore, the extent of the "limiting fragmentation region" grows significantly with increasing energy and at $\sqrt{s}$=200 GeV it extends more than two units away from the beam rapidity. This result is in contrast to the boost-invariance scenario [3] which predicts a broad plateau at mid-rapidity growing in extent with increasing beam energy. The measured pseudorapidity distributions appear to be dominated by two "fragmentation" regions, whose extent increases with collision energy. It can also be seen in fig. 5 that the "limiting curve" is different between central (top panels) and peripheral (bottom panels) collisions.
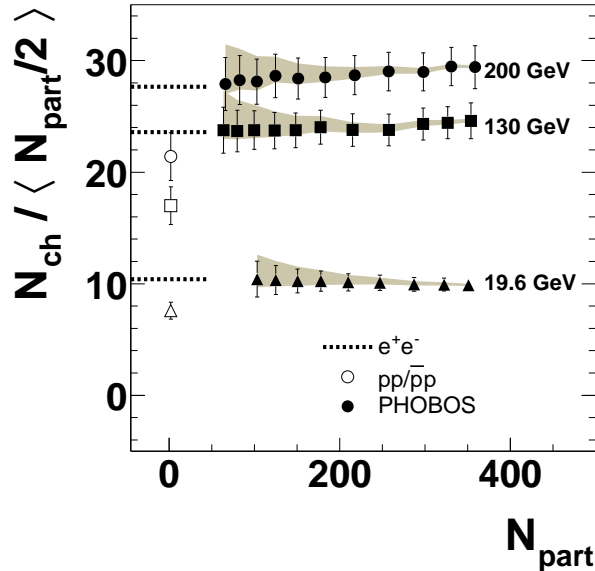
Figure 6: Centrality dependence of the total charged multiplicity per participant pair as measured by PHOBOS experiment at $\sqrt{s}$=19.6, 130 and 200 GeV (taken from [29]).

3.4 Integrated particle yield

The total number of charged particle is calculated by extrapolating the measured $dN_{\mathrm{ch}}/d\eta$ distributions over the full solid angle. In the case of PHOBOS experiment, which covers the pseudorapidity region $|\eta| < 5.4$, the extrapolation is quite small even at the highest RHIC energy. On the contrary, in the case of NA50, only $\approx$50% of the particles are in the acceptance of the multiplicity detector.

3.4.1 Scaling with centrality

The total charged particle yield per participant pair obtained by PHOBOS by integrating the measured $dN_{\mathrm{ch}}/d\eta$ distributions is shown in fig. 6 for different centrality bins at three different RHIC energies. Contrarily to the particle yield at mid-rapidity, the total charged-particle multiplicity results to be proportional to the number of participant nucleons at all three energies from $\sqrt{s}$=19.6 to 200 GeV. This N_{part} scaling comes from a compensation between the narrowing of the $dN_{\mathrm{ch}}/d\eta$ distributions and the more than linear increase of $dN/d\eta \mid_{\mathrm{max}}$ with increasing centrality. Furthermore, it can be seen that the charged multiplicity per participant pair in Au-Au collisions at RHIC agrees with the one measured in e^+e^- (and not in pp($\bar{\mathrm{p}}$)) collisions at the same energy.

3.4.2 Scaling with energy

The total charged multiplicity per participant pair as measured in central collision at AGS, SPS and RHIC experiments is shown in fig. 7 together with the same quantity from pp($\bar{\mathrm{p}}$)
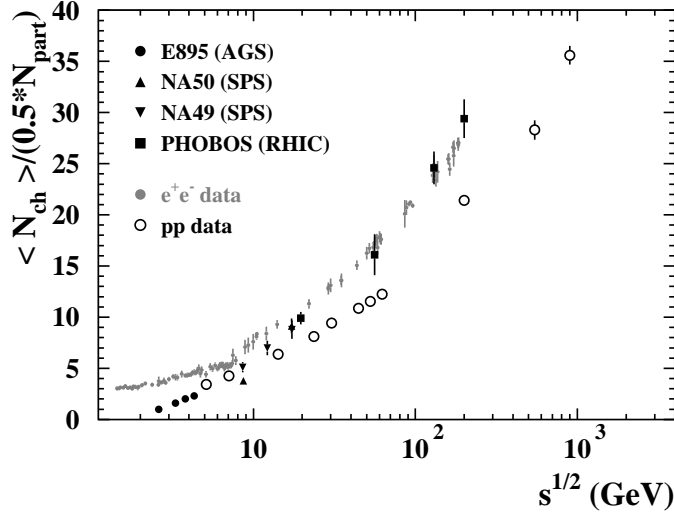
Figure 7: Energy dependence of the total charged multiplicity per participant pair for the most central ion-ion collisions from AGS to RHIC. pp($\bar{\text{p}}$) and e^+e^- data are superimposed.

and e^+e^- collisions.

The fact that pp($\bar{\text{p}}$) multiplicities lie about 30% below the e^+e^- data at the same energy can possibly be explained by the "leading particle effect": the outgoing proton carries away a substantial amount of the beam energy, thus reducing the energy effectively available for particle production [30]. It is observed that the multiplicities measured in pp($\bar{\text{p}}$) and e^+e^- reactions become consistent over a broad energy range if the effective energy $\left(\sqrt{s_{eff}} = \sqrt{s}/2\right)$ is introduced for pp($\bar{\text{p}}$) collisions to account for the leading particle effect.

Heavy ion multiplicities do not follow the e^+e^- trend over the whole $\sqrt{s}$ range. Instead, they lie below the pp($\bar{\text{p}}$) data at AGS energies, cross through the pp($\bar{\text{p}}$) curve around $\sqrt{s} \sim 10$ GeV and then gradually join the e^+e^- trend above the SPS energies. At RHIC energies, the multiplicity per participant pair in heavy-ion collisions agrees with the one observed in e^+e^- reactions at the same $\sqrt{s}$, suggesting a substantially reduced leading particle effect in central collisions of heavy nuclei at high energy [29]. The "suppression" of A-A multiplicity with respect to e^+e^- at low energies is possibly explained by the larger number of baryons produced at such energies which tend to suppress the overall multiplicity, due to the fact that the baryon chemical potential reduces the entropy [28]. These considerations suggest that the total multiplicity per participant pair might be a universal function of the available energy, irrespectively of the colliding system.

4 Perspectives for ALICE at the LHC

The predictions for the charged multiplicity at mid-rapidity in a central Pb-Pb collision at the LHC ($\sqrt{s}$ = 5.5 TeV) before RHIC startup varied between 2000 and 10000 particles per unit of pseudorapidity. At that time, therefore, ALICE [31] detectors were designed for optimal performance up to $dN/d\eta \mid_{\max} \approx 5000$ and reliable performance for $dN/d\eta \mid_{\max}$ up to 8000.

The wealth of multiplicity measurements which meanwhile became available from SPS and RHIC showed that the increase of multiplicity with increasing $\sqrt{s}$ was less dramatic than expected. Extrapolations of the presently available $dN/d\eta \mid_{\max}$ values measured in central collisions at AGS, SPS and RHIC (see fig. 3) would give for LHC energy values in the range between 1100 and 2000 particles per rapidity unit depending on the assumption on the $\sqrt{s}$ dependence of $dN/d\eta \mid_{\max}$. However, given the large energy gap between top RHIC and LHC energies, a dramatic change in the balance between particle production mechanisms is predicted to occur: multiplicities higher than the ones obtained from a simple extrapolation of RHIC data could be observed at the LHC due to a large contribution from mini-jets and hard scatterings.

Various detectors of the ALICE setup can be used to measure the charged particle multiplicity and to reconstruct the $dN_{\mathrm{ch}}/d\eta$ distributions over a wide η range. Different detecting and analysis techniques will therefore be used.

In the central rapidity region the $dN_{\mathrm{ch}}/d\eta$ distributions can be efficiently reconstructed using the two innermost layers of the Inner Tracking System (ITS) [32] which consist of two cylindrical layers of Silicon Pixel Detectors (SPD) with a length along the beam axis of 28.2 cm and radii of 4 cm (layer 1) and 7.2 cm (layer 2) respectively. These detectors will operate close to the beam pipe, in a region where the track density could be as high as 80 tracks per cm^2. The pixel size is 50μm in the rφ direction and 425 μm along the beam axis, resulting in $\approx$ 9.8 million channels which provide a binary (hit/no hit) information. Such a high segmentation allow to keep the occupancy below 1.5% for layer 1 and below 0.4% for layer 2 also in the case of 8000 charged particles in the central unit of η. The SPDs are the detectors of the ALICE barrel which provide the wider η coverage in the region around mid-rapidity ($|\eta| < 2$ for layer 1, $|\eta| < 1.4$ for layer 2).

Two different methods to estimate charged-particle multiplicity from SPD are considered. The first one consists in counting the number of "clusters" on each of the two SPD layers, the second in counting the number of "tracklets" obtained by associating clusters in the two layers. The performances of these methods have been evaluated by means of Monte Carlo simulations based with a detailed description of the detector geometry. The reconstructed values of $dN/d\eta \mid_{\max}$ by counting clusters on layer 1 are found to reproduce the generated values for $dN/d\eta \mid_{\max} \leq 5000$, while for higher multiplicities cluster merging effects lead to an underestimation of the number of generated particles. The $dN_{\mathrm{ch}}/d\eta$ reconstruction based on counting clusters on layer 2 suffers from secondary production in the inner layer and consequently gives an overestimation of the generated multiplicity. The "tracklet" method has the advantage of allowing for an efficient background rejection (noise, secondary particles) by defining appropriate $\Delta\eta$ and $\Delta\varphi$ windows for the cluster association. The drawback is a
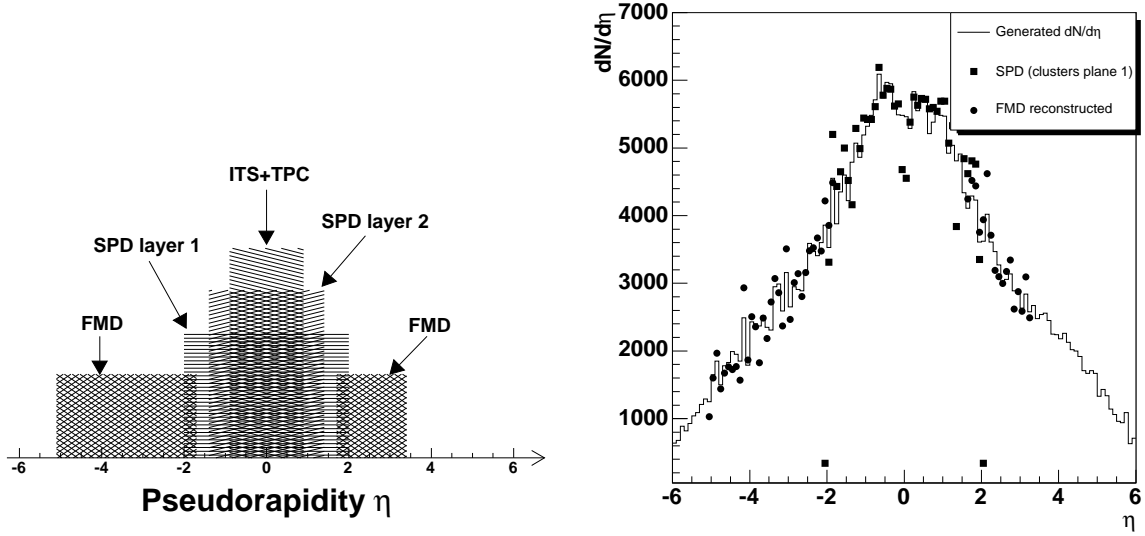
Figure 8: Left panel: pseudorapidity coverage of the ALICE detectors used in multiplicity measurements. Right panel: η distribution of charged particles reconstructed in the ITS and FMD detectors for a central HIJING event.

significant decrease of the overall efficiency (see [33] for details), which should be corrected on the basis of Monte Carlo simulations.

The magnetic field affects mostly the number of clusters in the second layer and consequently the number of found tracklets decreases with increasing field strength. This is mainly due to the tracks of very low momentum which are unable to hit the second layer of SPD. In principle, a special running session with the magnetic field off will offer the best configuration for the multiplicity measurement.

A more refined multiplicity measurement in the central barrel could be obtained with track reconstruction using all the six layers of the ITS, the Time Projection Chamber (TPC) and the Transition Radiation Detector (TRD) at the price of a smaller pseudorapidity coverage (($|\eta| < 0.9$) and a longer analysis time due to stricter requirements on alignment and detector calibration.

In the forward and backward regions, the multiplicity will be measured by the Forward Multiplicity Detectors (FMD) which are 5 silicon strip ring counters with 51200 channels covering the regions $-5.1 < \eta < -1.7$ and $1.7 < \eta < 3.4$. Due to the high occupancy expected for central Pb-Pb interactions (up to 2.2 particles per pad for $dN/d\eta \mid_{\max}=6000$) it will not be possible to determine the number of charged particles by simply counting the pads which have fired, due to the large contribution of channels with more than one incident particle. Charged multiplicity will be therefore estimated from the measurement of the total energy deposited in each pad. An alternative method based on counting empty pads and extracting from it the number of incident particles assuming Poisson statistics has also been developed.

13

The ITS and FMD detectors will allow to measure charged particles over a wide (about 8 η-units) pseudorapidity region, as it can be seen in fig. 8 (left). It should be noted that the acceptances quoted in this plot are referred to the nominal vertex position and that the spread of the vertex position along the beam direction will allow to extend the η coverage. In fig. 8 (right) the generated and reconstructed $dN_{\mathrm{ch}}/d\eta$ pseudorapidity distributions of charged particles for a single central HIJING event are shown. One can see that even for a single event the accuracy on the multiplicity determination, when using a bin width of 0.1 η-units, is of the order of 7%. The few bins in the ITS acceptance regions where one observes a clear underestimation of the multiplicity are simply due to the geometrical junctions of the modules of the SPD.

Acknowledgments

References

[1] Bialas, Bleszynski and Czyz, Nucl. Phys. B 111 (1976), 461.

[2] R. J. Glauber, Lectures in Theoretical Physics, NY, 1959, Vol. 1, 315.

[3] J.D. Bjorken, Phys. Rev. D 27 (1983), 140.

[4] J. Benecke et al., Phys. Rev. 188 (1969) 2159.

[5] M.C. Abreu et al. (NA50 coll.), Phys. Lett. B 530 (2002), 33.

[6] B. B. Back et al. (PHOBOS coll.), Phys. Rev. Lett. 87 (2001), 102203.

[7] F. Antinori et al. (NA57 coll.), J. Phys. G 31 (2005), 321.

[8] I. G. Bearden et al. (BRAHMS coll.), Phys. Lett. B523 (2001), 227.

[9] I. G. Bearden et al. (BRAHMS coll.), Phys. Rev. Lett. 88 (2002), 202301.

[10] B. B. Back et al. (PHOBOS coll.), Phys. Rev. Lett. 85 (2000), 3100.

[11] K. Adkox et al. (PHENIX coll.), Phys. Rev. Lett. 86 (2001), 3500.

[12] H. Appelshäuser et al (NA49 coll.), Phys. Rev. Lett. 82 (1999), 2471.

[13] C. Adler et al. (STAR coll.), Phys. Rev. Lett. 87 (2001) 112303.

[14] M.C. Abreu et al. (NA50 coll.), Phys. Lett. B 530 (2002), 43.

[15] M.M. Aggarwal et al (WA98 coll.), Eur. Phys. J. C18 (2001) 651.

[16] K. Werner, *Phys. Rep.* **232** (1993) 87.

[17] B. B. Back et al (PHOBOS coll.), Phys. Rev. C70 (2004) 021902(R).

[18] X. Wang and M. Gyulassy, Comp. Phys. Comm. 83 (1994) 307.

[19] D. Kharzeev and M. Nardi, Phys. Lett. B507 (2001) 121.

[20] D. Kharzeev and E. Levin, Phys. Lett. B523 (2001) 79.

[21] J. Adams et al. (STAR coll.), Nucl. Phys. A757 (2005) 102.

[22] B. B. Back et al (PHOBOS coll.), nucl-ex/0509034.

[23] K.Adkox et al. (PHENIX coll.), Nucl. Phys. A757 (2005) 184.

[24] T. Abbott et al. (E802 coll.), Phys. Rev. C45 (1992), 2933.

[25] B. B. Back et al. (PHOBOS coll.), Phys. Rev. Lett. 91 (2003) 052303.

[26] M.I. Adamovich et al., Nucl. Phys. A566 (1994), 419c. and C. Höhne et al. (NA49 coll.), Nucl. Phys. A661 (1999) 485c.

[27] P. Senger and H. Ströbele, J. Phys. G 25 (1999), R59.

[28] B. B. Back et al. (PHOBOS coll.), Nucl. Phys. A757 (2005) 28.

[29] B. B. Back et al nucl-ex/0301017 v1

[30] M. Basile et al., Phys. Lett. B95 (1980) 311.

[31] ALICE Collaboration, Technical proposal, CERN/LHCC 95-71.

[32] ALICE Collaboration, Technical Design Report of the Inner Tracking System, CERN/LHCC 1999-12.

[33] ALICE Collaboration, Physics Performance Report, vol. II.